A Variationally Computed $T = 300$ K Line List for NH_3[†]

Sergei N. Yurchenko,[||] **Robert J. Barber,**[‡] **Andrey Yachmenev,**[¶] **Walter Thiel,**[¶] **Per Jensen,**[§] **and Jonathan Tennyson*,**[‡]

Institut für Physikalische Chemie und Elektrochemie, Technische Universität Dresden, D-01062 Dresden, Germany, Department of Physics and Astronomy, University College London, London WC1E 6BT, U.K., Max-Planck-Institut für Kohlenforschung, Kaiser-Wilhelm-Platz 1, D-45470 Mülheim an der Ruhr, Germany, and FBC, Theoretische Chemie, Bergische Universität, D-42097 Wuppertal, Germany

Calculations are reported on the rotation−vibration energy levels of ammonia with associated transition intensities. A potential energy surface obtained from coupled cluster CCSD(T) calculations and subsequent fitting against experimental data is further refined by a slight adjustment of the equilibrium geometry, which leads to a significant improvement in the rotational energy level structure. A new accurate ab initio dipole moment surface is determined at the frozen core CCSD(T)/aug-cc-pVQZ level. The calculation of an extensive ammonia line list necessitates a number of algorithmic improvements in the program TROVE that is used for the variational treatment of nuclear motion. Rotation−vibration transitions for $^{14}NH_3$ involving states with energies up to 12000 cm^{-1} and rotational quantum number $J = 20$ are calculated. This gives 3.25 million transitions between 184400 energy levels. Comparisons show good agreement with data in the HITRAN database but suggest that HITRAN is missing significant ammonia absorptions, particularly in the near-infrared.

1. Introduction

Polyatomic molecules with large-amplitude motions have complex spectra, and some of these are well-suited to probing the physical conditions of astrophysical objects. $^{14}NH_3$ (henceforth referred to as ammonia or NH_3) is the best tetratomic example of such a molecule. It is present in a wide range of astrophysical environments, and because of the richness and intensity of its spectrum, it is easily observed from Earth. The positions of many of the stronger NH_3 lines have been measured and the transitions assigned. Some of these lines are regularly used to determine temperatures and molecular number densities in distant objects.

For example, ammonia is the main nitrogen-containing molecule observable in the spectra of cometary coma, and its number density in this region is typically ∼0.5% of that of gaseous H_2O.[1] The atmosphere of Jupiter also contains ammonia,[2,3] and a notable feature during the impact of Comet Shoemaker−Levy 9 with Jupiter in 1994 was an enhancement in the concentration of NH_3 gas in the planet's stratosphere over the impact sites.[4] Ortho−para ratio measurements have been used to measure the nuclear spin temperature of gaseous NH_3 in the comas of C/2001 Neat,[5] 9P/Tempel 1,[6] and other comets.

The spectra of M- and L-type brown dwarfs are dominated by H_2O. CH_4 becomes more important in the atmospheres of later-type dwarfs, and by the mid T-type, NH_3 absorption is significant, particularly in the 10.5 μm region.[7,8] Modeling suggests that ammonia will be an even more important source of opacity in the yet-to-be discovered Y-dwarfs,[9] and conse-

quently, it is anticipated that NH_3 absorption bands will be the signature of this new class of ultracool dwarf.

Ammonia is also predicted to be observable in the atmospheres of extrasolar giant planets (EGPs).[10] The reactions by which N_2 and H_2 are converted into ammonia in the atmospheres of brown dwarfs and planets are complex and outside of the scope of this paper. However, the equilibrium between N_2 and NH_3 favors NH_3 at lower temperatures as (to a lesser extent) do higher pressures. These temperature and pressure dependencies suggest that the outer atmospheres of EGPs at large orbital distances will contain significant quantities of ammonia.[10] Unlike CH_4, which is also predicted to be present in the outer atmospheres of EGPs and which has been inferred in HD 189733b,[11] NH_3 has not yet been detected in the atmosphere of any exoplanet.

One impediment to identifying and interpreting NH_3 features in the spectra of astrophysical objects is the fact that the vast majority of lines in the NH_3 spectrum are not known. The HITRAN database[12] encapsulates the knowledge of ammonia rotation−vibration spectra, yet about half of the transitions in the database remain unassigned, and as we demonstrate below, many important frequency regions are simply absent. For simulations of hot spectra, the situation is even worse, and it is not realistic to expect this situation to be resolved experimentally. Accurate first-principles quantum mechanical calculations would therefore appear to be the solution to this problem. However, since such calculations are extremely challenging, no line list currently exists that is complete or accurate enough to be used to model and interpret NH_3 data from any environment where the temperature is above 400 K.

Previous studies[13−20] have solved the nuclear motion problem for NH_3 on high-level ab initio coupled cluster potential energy surfaces and compared the resulting energy levels against experimental data. In some cases,[21,22] the corresponding wave functions for nuclear motion have been employed, in conjunction

with ab initio dipole moment surfaces, to calculate the intensity of some of the lines in a small number of rovibrational bands. However, in every case, such work has been performed within very constrained parameters. The energy levels computed are numbered in the hundreds, giving rise to a few thousand transitions between these levels. The present state of the work on the ammonia problem prior to the current paper has recently been summarized in more detail by Huang et al.[20] After submission of this paper, vibrational term values were reported[23] for NH_3 using an exact variational nuclear motion treatment in combination with one of our previously published potential energy surfaces.[19]

From an astrophysical perspective, the absence of a satisfactory ammonia line list means that it is not possible to model accurately the atmospheres of late brown dwarfs or the cooler classes of exoplanets, environments where ammonia is a major source of opacity. Our aim is to provide a 1500 K line list for NH_3 (henceforth referred to as the high-temperature line list) that will fill this important gap. There are three elements in the generation of an ab initio line list, accurate potential energy and dipole moment surfaces (PES and DMS, respectively) and a computer program to generate accurate wave functions and eigenvalue solutions for the nuclear Schrödinger equation and associated transition intensities. Here, we test these three elements to produce an actual ammonia line list, albeit one that is less complete and accurate than our eventual goal. However, this list will be useful for generating room-temperature spectra. It is this shorter NH_3 line list (subsequently referred to as a cool line list) that we present in the current paper, together with the implications of this work for the subsequent production of a high-temperature, or hot, line list.

We adopt a variational approach to solving the nuclear motion Schrödinger equation. Our initial calculations used the program XY3[21,24] to compute spectral line intensities for a number of pyramidal molecules[21,22,25,26] and to simulate their rovibrational bands, for example, in the NH_3 absorption spectra at 300 K.[22] The theoretical results were generally in very good agreement with experiment. However, these XY3 computations proved to be quite demanding in terms of both processor time and memory requirements, and it was clear that a more efficient computational tool would be required for the hot line list. Here, we therefore employ the recently developed program TROVE,[27] which implements a general variational approach for calculating the rovibrational spectra of small polyatomic molecules. We develop intensity and symmetrization tools specific to the NH_3 problem and introduce a number of algorithmic improvements that make the calculations more tractable. We present extracts from the cool ammonia line list produced using TROVE and discuss their accuracy and the associated computational costs.

2. The Ammonia Molecule and Its Quantum Numbers

Ammonia is a symmetric top molecule. Its equilibrium geometry is a regular pyramid; the three hydrogen nuclei are at the corners of an equilateral triangle, and the nitrogen nucleus is located on the axis of symmetry, which is perpendicular to the plane of the hydrogen nuclei. The molecule is capable of inversion, that is to say, the nitrogen nucleus is able to take up positions on either side of the plane of the hydrogen nuclei.

Nine parameters are required to define the internal rovibrational motion of a tetratomic molecule. There are six vibrational modes (of which, in the case of NH_3, two are doubly degenerate). The standard Herzberg convention[28] labels the symmetric stretch and symmetric bend as ν_1 and ν_2, respectively, and the asymmetric stretch and asymmetric bend as ν_3 and ν_4, respec-

tively. These last two are degenerate and consequently carry additional quantum numbers in the form of the suffixes l_3 and l_4, respectively. The total angular momentum is J, and K is its projection on the molecular symmetry axis. The ninth quantum number Γ is the total symmetry in the molecular symmetry group[29] $D_{3h}(M)$, to which NH_3 belongs. The rigorous selection rules which determine the allowed electric dipole transitions of NH_3 are $\Delta J = J' - J'' = 0, \pm 1$ ($J'' + J' \geq 1$), with symmetry selection rules $A'_1 \not\leftrightarrow A''_1$, $A'_2 \leftrightarrow A''_2$, and $E' \leftrightarrow E''$.

We use a unique "local mode" representation that is particularly suited to our choice of internal coordinates for the primitive 1D basis functions $\phi_{n_i}(\xi)$. Apart from the general quantum numbers associated with the molecular group symmetry Γ and total angular momentum J, our quantum numbers are Γ_{rot}, K, τ_{rot}, Γ_{vib}, n_1, n_2, n_3, n_4, n_5, and n_6. Here, J, K, and Γ are as above, and n_1, n_2, n_3 are stretching local mode quantum numbers[30] which correlate with the normal mode notation as $n_1 + n_2 + n_3 = \nu_1 + \nu_3$; n_4 and n_5 are deformational bending quanta, and n_6 is the inversion quantum number equivalent to $2\nu_2 + \tau_{inv}$, where ν_2 is the normal mode quantum number and $\tau_{inv} = n_6 \bmod 2$ is the inversion parity.[24] Finally, Γ_{rot} and Γ_{vib} are the rotational and vibrational symmetry in $D_{3h}(M)$.

Our deformational band quantum numbers n_4 and n_5 are not the standard ν_4 and l_4 quantum numbers (because of the way the basis is constructed, they are more local mode); the correlation of ν_4 is straightforward, $n_4 + n_5 = \nu_4$, while assigning l_4 values is more tricky since there is no separate, identifiable vibrational symmetry to start with. This leads to the same ν_4 quantum numbers as an experimentalist would have assigned from looking at regularities in the spectrum. Therefore, most of the time, one obtains a labeling that makes it easy to communicate with experimentalists. When there is strong interaction between basis states, the labeling becomes problematic, but it is a question of whether such states really have defined ν_4 and l_4 quantum numbers.

In the approximation that the vibration and rotation motions are entirely separated, simple arguments can be used to rationalize the molecular spectra. In this case, the states having different values of K are not mixed, which gives rise to the concept of a good quantum number K[29] and approximate dipole selection rules $\Delta K = 0$ through the component of the electric dipole moment parallel to the symmetry axis. This, for example, results in rapid decay of the states with higher values of K (typically in less than $\sim$100 s) via $\Delta J = 1$ transitions, while states with lower K values, so-called metastable states, decay very slowly (typically having a lifetime of $\sim 10^9$ s) as they rely on small dipole moments perpendicular to the symmetry axis that arise due to the interaction of rotational and vibrational motions.

The vibrational ground state of ammonia is split into two states, the lowest-energy 0^- state lying 0.793 cm^{-1} above the lowest 0^+ state. Therefore, the (almost) uniformly spaced pure rotational lines (which are in the submillimeter and far-IR regions) have two components, separated by the energy difference between the 0^- and 0^+ states. Transitions can also occur between the $+$ and $-$ rotational states. These are governed by approximate selection rules, $\nu^+ \leftrightarrow \nu^-$, $\Delta J = 0$, and $\Delta K = 0$ ($K \neq 0$), and give rise to a large number of lines in the 1.25 cm^{-1} (24 GHz) region. These have been seen experimentally,[31,32] and observations at 23.6 GHz of the NH_3 $J = 1$, $K = 1$ inversion transition[33] resulted in ammonia being the first polyatomic molecule to be recorded in the interstellar medium.

Because of the different relative spin orientations of the three hydrogen nuclei, the NH_3 molecule has two distinct species,

ortho and para. *ortho*-NH$_3$ has all three hydrogen spins parallel, a consequence of which is that the angular momentum quantum number K can only take on values equal to $3n$, where n is an integer. *para*-NH$_3$ has one antiparallel hydrogen spin, which gives rise to all other values of K.

Our variational calculations do not use approximate quantum numbers or approximate selection rules. However we employ the concept of near quantum numbers,[29] which is based on the idea of assigning the calculated eigenfunctions according to the largest contribution in its expansion.[29] This is important for correlating the theoretical and experimental spectral information and is performed automatically.

3. The Dipole Moment Surface

The ab initio dipole moments employed in the present work were computed with the MOLPRO2000[34,35] package at the CCSD(T)/aug-cc-pVQZ level of theory (i.e., coupled cluster theory with all single and double substitutions[36] and a perturbative treatment of connected triple excitations[37] with the augmented correlation-consistent quadruple-ζ basis[38,39]) in the frozen core approximation. We refer to this method and basis set as the AQZfc level of theory. Dipole moments were computed in a numerical finite difference procedure with an added external dipole field of 0.005 au.

The ab initio dipole moment surface (DMS) was determined on a six-dimensional grid consisting of 4677 geometries with coordinates in the ranges of $0.9 \leq r_1 \leq r_2 \leq r_3 \leq 1.20$ Å and $80 \leq \alpha_1, \alpha_2, \alpha_3 \leq 120°$. Here, r_i is the instantaneous value of the internuclear distance N$-$H$_i$, $i = 1, 2, 3$, and the bond angles are given as $\alpha_1 = \angle(H_2NH_3)$, $\alpha_2 = \angle(H_1NH_3)$, and $\alpha_3 = \angle(H_1NH_2)$.

It is necessary to express the DMS analytically in terms of the internal coordinates of the molecule. Earlier work[22] used an extended version of the molecular bond (MB) representation. For NH$_3$, the dipole moment vector is given in the MB representation as

$$\bar{\mu} = \bar{\mu}_1^{\text{Bond}}\mathbf{e}_1 + \bar{\mu}_2^{\text{Bond}}\mathbf{e}_2 + \bar{\mu}_3^{\text{Bond}}\mathbf{e}_3 \qquad (1)$$

Here, each unit vector $\mathbf{e}_i$ lies along one of the N$-$H$_i$ bonds

$$\mathbf{e}_i = \frac{\mathbf{r}_i - \mathbf{r}_4}{|\mathbf{r}_i - \mathbf{r}_4|} \qquad (2)$$

with $\mathbf{r}_i$ as the position vector of nucleus i (the protons are labeled as 1, 2, 3, and the nitrogen nucleus is labeled 4). The functions $\bar{\mu}_i^{\text{Bond}}$, $i = 1, 2, 3$, in eq 1 depend on the vibrational coordinates and are expressed[22] in terms of the dipole moment projections $(\bar{\mu} \cdot \mathbf{e}_j)$ onto the bonds of the molecule.

A disadvantage of the MB representation is the ambiguity at and near planar geometries when the three vectors $\mathbf{e}_i$ become linearly dependent, or nearly linearly dependent, and singularities appear in the determination of the $\bar{\mu}_i^{\text{Bond}}$ functions. We have overcome this problem by reformulating the $\bar{\mu}_i^{\text{Bond}}$ functions in terms of symmetry-adapted combinations of the MB projections $(\bar{\mu} \cdot \mathbf{e}_j)$

$$\bar{\mu}_{A_1''}^{\text{SMB}} = (\bar{\mu} \cdot \mathbf{e}_N) \qquad (3)$$

$$\bar{\mu}_{E_a'}^{\text{SMB}} = \frac{1}{\sqrt{6}}[2(\bar{\mu} \cdot \mathbf{e}_1) - (\bar{\mu} \cdot \mathbf{e}_2) - (\bar{\mu} \cdot \mathbf{e}_3)] \qquad (4)$$

$$\bar{\mu}_{E_b'}^{\text{SMB}} = \frac{1}{\sqrt{2}}[(\bar{\mu} \cdot \mathbf{e}_2) - (\bar{\mu} \cdot \mathbf{e}_3)] \qquad (5)$$

where we have introduced an additional reference MB vector $\mathbf{e}_N = \mathbf{q}_N/|\mathbf{q}_N|$ defined by means of the trisector

$$\mathbf{q}_N = (\mathbf{e}_1 \times \mathbf{e}_2) + (\mathbf{e}_2 \times \mathbf{e}_3) + (\mathbf{e}_3 \times \mathbf{e}_1) \qquad (6)$$

This symmetrized molecular bond representation (denoted as SMB) has been used by Yurchenko et al.[22] to resolve a similar issue encountered in connection with representing the polarizability tensor of NH$_3^+$ in terms of analytical functions. The subscripts of the $\bar{\mu}_\Gamma^{\text{SMB}}$ functions ($\Gamma = A_1''$, E$_a'$, E$_b'$) in eqs 3$-$5 refer to irreducible representations[29] of D_{3h}(M); $\bar{\mu}_{A_1''}^{\text{SMB}}$ has A_1'' symmetry in D_{3h}(M), and $(\bar{\mu}_{E_a}^{\text{SMB}}, \bar{\mu}_{E_b}^{\text{SMB}})$ transform as the E$'$ irreducible representation. The symmetrized vectors

$$\mathbf{e}_{A_1'} = \mathbf{e}_N \qquad (7)$$

$$\mathbf{e}_{E_a''} = \frac{1}{\sqrt{6}}(2\mathbf{e}_1 - \mathbf{e}_2 - \mathbf{e}_3) \qquad (8)$$

$$\mathbf{e}_{E_b''} = \frac{1}{\sqrt{2}}(\mathbf{e}_2 - \mathbf{e}_3) \qquad (9)$$

have A_1' and E$''$ symmetry in the same manner.

The dipole moment vector $\bar{\mu}$ vanishes at symmetric, planar configurations of D_{3h} geometrical symmetry. Also, the $\bar{\mu}_{A_1''}^{\text{SMB}}$ component is antisymmetric under the inversion operation E^{*}[29] and vanishes at planarity, which leaves only two independent components of $\bar{\mu}$ at planarity.

The advantage of having a DMS representation in terms of the projections $(\bar{\mu} \cdot \mathbf{e}_j)$ is that it is body-fixed in the sense that it relates the dipole moment vector directly to the instantaneous positions of the nuclei (i.e., to the vectors $\mathbf{r}_i$). These projections are well-suited to being represented as analytical functions of the vibrational coordinates.[21] For intensity simulations, however, we require the Cartesian components $\bar{\mu}_\alpha$, $\alpha = x, y, z$, of the dipole moment along the molecule-fixed xyz axes. These can be obtained by inverting the linear equations

$$\bar{\mu}_\Gamma^{\text{SMB}} = \sum_{\alpha = x,y,z} A_{\Gamma,\alpha}\bar{\mu}_\alpha \qquad (10)$$

where $A_{\Gamma,\alpha}$ is the α-coordinate ($\alpha = x, y, z$) of the vector $\mathbf{e}_\Gamma$ ($\Gamma = A_1'$, E$_a$, E$_b$) in eqs 7$-$9. When the molecule is planar, $\bar{\mu}_{A_1'}^{\text{SMB}}$ is zero, as is the corresponding right-hand side in eq 10. Thus, at planar configurations, the system of linear equations in $\bar{\mu}_\alpha$ contains two nontrivial equations only. At near-planar configurations, $\bar{\mu}_{A_1'}^{\text{SMB}}$ is not exactly zero and cannot be neglected, and therefore, eq 10 becomes near-linear-dependent. The symmetry-adapted representation of eqs 3$-$5 appears to be well-defined even for these geometries, at least in connection with the LAPACK solver DGELSS, which can handle such rank-deficient equation systems in a least-squares approach.[40]

In the SMB theory, the functions $\bar{\mu}_\Gamma^{\text{SMB}}$ (henceforth referred to as $\bar{\mu}_\Gamma$) are now represented as expansions

$$\bar{\mu}_{A_1''} = \cos \bar{\rho} [\mu_0^{(A_1'')} + \sum_k \mu_k^{(A_1'')} \xi_k + \sum_{k,l} \mu_{k,l}^{(A_1'')} \xi_k \xi_l +$$
$$\sum_{k,l,m} \mu_{k,l,m}^{(A_1'')} \xi_k \xi_l \xi_m + ...] \quad (11)$$

$$\bar{\mu}_{E_a'} = \mu_0^{(E_a')} + \sum_k \mu_k^{(E_a')} \xi_k + \sum_{k,l} \mu_{k,l}^{(E_a')} \xi_k \xi_l +$$
$$\sum_{k,l,m} \mu_{k,l,m}^{(E_a')} \xi_k \xi_l \xi_m + ... \quad (12)$$

$$\bar{\mu}_{E_b'} = \mu_0^{(E_b')} + \sum_k \mu_k^{(E_b')} \xi_k + \sum_{k,l} \mu_{k,l}^{(E_b')} \xi_k \xi_l +$$
$$\sum_{k,l,m} \mu_{k,l,m}^{(E_b')} \xi_k \xi_l \xi_m + ... \quad (13)$$

in terms of the variables

$$\xi_k = (r_k - r_e) \exp[-\beta(r_k - r_e)^2] \quad k = 1, 2, 3$$
$$(14)$$

which describe the stretching motion

$$\xi_4 = \frac{1}{\sqrt{6}} (2\alpha_1 - \alpha_2 - \alpha_3) \quad (15)$$

$$\xi_5 = \frac{1}{\sqrt{2}} (\alpha_2 - \alpha_3) \quad (16)$$

which describe the "deformation" bending, and

$$\xi_6 = \sin \bar{\rho}_e - \sin \bar{\rho} \quad (17)$$

which describes the out-of-plane bending motion. In eq 17

$$\sin \bar{\rho} = \frac{2}{\sqrt{3}} \sin[(\alpha_1 + \alpha_2 + \alpha_3)/6] \quad (18)$$

and $\sin(\bar{\rho}_e)$ is the equilibrium value of $\sin(\bar{\rho})$. The factor $\cos \bar{\rho}$ $= \pm(1 - \sin^2\bar{\rho})^{1/2}$ in eq 11 ensures that the dipole moment function $\bar{\mu}_{A_1''}$ changes sign when $\bar{\rho} = 0, ..., \pi$ is changed to $\pi - \bar{\rho}$. Following Marquardt et al.,[41] we have introduced the factor $\exp[-\beta(r_k - r_e)^2]$ in eq 14 in order to keep the expansion in eq 13 from diverging at large r_i.

Because of the symmetry requirements, not all of the expansion parameters $\mu_{k,l,m,...}^{(\Gamma)}$ are independent. The two E′ symmetry components $\bar{\mu}_{E_a'}$ and $\bar{\mu}_{E_b'}$ have related parameter values, while $\bar{\mu}_{A_1''}$ is "independent" of them. Yurchenko et al.[21] define a set of independent parameters $\mu_{k,l,m,...}^{(\Gamma)}$ and derive symmetry relations determining the remaining parameter values; we use these results in the present work. The expansions in eqs 11−13 are truncated after the fourth-order, which corresponds to 109 independent parameters for $\bar{\mu}_{A_1''}$ and 146 independent parameters for $(\bar{\mu}_{E_a'}, \bar{\mu}_{E_b'})$. We were able to usefully vary 176 parameters $\mu_{k,l,m,...}^{(\Gamma)}$ in a least-squares fitting to the ab initio dipole moment data, and the resulting root-mean-square (rms) error was 0.00035 D. The parameters $\mu_{k,l,m,...}^{(\Gamma)}$ together with the Fortran routine for calculating the dipole moment components are provided as

Supporting Information. The new ab initio dipole moment function will be referred to as AQZfc.

For the "equilibrium" dipole moment, we obtained $\mu_e = -\bar{\mu}_{A_1''}$ = 1.5148 D, based on the ab initio equilibrium geometry of r_1 = $r_2 = r_3 = r_e = 1.0103$ Å and $\alpha_1 = \alpha_2 = \alpha_3 = \alpha_e = 106.72°$.[14] This is very similar to the ATZfc DMS value of 1.5198 D.[22] The experimental value for μ_e is usually quoted as (1.561 ± 0.005) D.[42] The large discrepancy between this experimental value and high-level ab initio results has been noted before.[43] It has been attributed to uncertainties in the conversion of the measured dipole moments of specific rovibrational states to an equilibrium value which may have led to an overestimate.[43] This view has been corroborated by a recent extensive ab initio study[44] which reported a best equilibrium dipole moment of 1.5157 D at the CCSD(T)/CBS+CV level (with complete basis set extrapolations and inclusion of core−valence corrections) and a zero-point-corrected ground-state dipole moment of 1.4764 D, close to the directly measured ground-state value of 1.471932(7) D.[45] Our AQZfc value for the vibrationally averaged ground-state dipole moment is 1.4638 D. This clearly indicates that the true equilibrium dipole moment of ammonia should be closer to 1.51 than 1.56 D.

4. The Intensity Simulations with TROVE

4.1. General Formulas. We require the line strengths (from which Einstein coefficients and absorption intensities can be computed) for all transitions between the rovibrational energy levels that satisfy the selection rules using the standard methodology.[46]

We consider a transition from an initial state i with rotation−vibration wave function $|\Phi_{rv}^{(i)}\rangle$ to a final state f with rotation−vibration wave function $|\Phi_{rv}^{(f)}\rangle$. The line strength[21,29,47] $S(f \leftarrow i)$ of the rotation−vibration transition f ← i (neglecting hyperfine structure) is obtained from[21]

$$S(f \leftarrow i) = g_{ns} \sum_{m_f, m_i} \sum_{A=X,Y,Z} |\langle \Phi_{rv}^{(f)} | \bar{\mu}_A | \Phi_{rv}^{(i)} \rangle|^2 \quad (19)$$

where g_{ns} is the nuclear spin statistical weight factor[29,47] and $\bar{\mu}_A$ is the electronically averaged component of the molecular dipole moment along the space-fixed axis $A = X$, Y, or Z. The quantum numbers m_i and m_f are the projections of the total angular momentum J, in units of $\hbar$, on the Z axis in the initial and final states, respectively.

Assuming the absorbing molecules to be in thermal equilibrium at an absolute temperature T, the absorption line intensity is determined by

$$I(f \leftarrow i) = \int_{Line} \varepsilon(\tilde{\nu}) d\tilde{\nu} = \frac{8\pi^3 N_A \tilde{\nu}_{if}}{(4\pi\varepsilon_0)3hc} \frac{e^{-E_i/kT}}{Q} \times$$
$$[1 - \exp(-hc\tilde{\nu}_{if}/kT)]S(f \leftarrow i) \quad (20)$$

Here $\varepsilon(\tilde{\nu})$ is the absorption coefficient,[29,47] $\tilde{\nu}$ is the absorption wavenumber, and eq 20 refers to the transition from the state i with energy E_i to the state f with energy E_f, where $hc\tilde{\nu}_{if} = E_f - E_i$. Q is the partition function defined as $Q = \sum_j g_j \exp(-E_j/kT)$, where g_j is the total degeneracy of the state with energy E_j and the sum runs over all energy levels of the molecule and the other symbols have their usual meanings. The total degeneracy g_j is given by $(2J + 1)$ times the nuclear spin degeneracy, which is 0, 12, 6, 0, 12, and 6 for A′$_1$, A′$_2$, E′, A″$_1$, A″$_2$, and E″ symmetries, respectively. Experimental values of

$I(\text{f} \leftarrow \text{i})$ are obtained by numerical integration of experimentally determined $\varepsilon(\tilde{v})$ values.

A detailed expression for the line strength of an individual rovibrational transition within an isolated electronic state of an XY$_3$ pyramidal molecule is given in eq 21 of Yurchenko et al.[21] Provided that the population of the lower (initial) state is defined by the Boltzmann distribution, it is sufficient to consider only transitions starting from the levels below $E_i^{\text{max}}/hc = 3200$ cm^{-1}, which corresponds in eq 20 to Boltzmann factors $\exp(-E_i/kT) > 2 \times 10^{-7}$ at $T = 300$ K. For similar reasons, the range of the rotational excitations can be safely limited by $J = 20$. The frequency range selected is 0–8000 cm^{-1}; the total energy limit (and the maximal energy for the final state) E^{max}/hc is 12000 cm^{-1}.

4.2. Computational Details. We use a symmetry-adapted basis set in the variational nuclear motion calculations. The Hamiltonian matrix is factorized into size-independent blocks according to $D_{3h}(\text{M})$ symmetry, A$_1'$, A$_2'$, E$_a'$, E$_b'$, A$_1''$, A$_2''$, E$_a''$, and E$_b''$. The A$_1'$ and A$_1''$ matrices are irrelevant for NH$_3$ as the corresponding states have zero nuclear spin statistical weights. Only one member of the pairs E$_a$ and E$_b$ needs to be processed as they represent doubly degenerate solutions. This provides a considerable savings in computing time since the dimensions of the E matrices are approximately twice as large as those of the A$_2$ matrices.

The calculation of the matrix elements $\langle \Phi_{\text{rv}}^{(\text{f})} | \bar{\mu}_A | \Phi_{\text{rv}}^{(\text{i})} \rangle$ in eq 19 proved to be a bottleneck. Here, the wave functions $\Phi_{\text{rv}}^{(\text{w})}$ are expressed as linear combinations of basis functions (see eq 65 of Yurchenko et al.[24])

$$|\Phi_{\text{rv}}^{(\text{w})}\rangle = \sum_{VK\tau_{\text{rot}}} C_{VK\tau_{\text{rot}}}^{(\text{w})} |J_{\text{w}} K m_{\text{w}} \tau_{\text{rot}}\rangle |V\rangle \qquad \text{w} = \text{i or f} \tag{21}$$

$C_{VK\tau_{\text{rot}}}^{(\text{w})}$ are expansion coefficients, $|J_{\text{w}} K m_{\text{w}} \tau_{\text{rot}}\rangle$ is a symmetrized rotational basis function, τ_{rot} ($=0$ or 1) determines the rotational parity as $(-1)^{\tau_{\text{rot}}}$, and $|V\rangle$ is a vibrational basis function. In order to speed up this part of the calculations, we applied a prescreening procedure to the expansion coefficients $C_{VK\tau_{\text{rot}}}^{(\text{f})}$.[22] All terms with coefficients less than the threshold value of 10^{-16} were excluded from the integration.

A further speedup was achieved by optimizing the strategy for calculating the line strengths, eq 19. The evaluation of the dipole moment matrix elements $\langle \Phi_{\text{rv}}^{(\text{f})} | \bar{\mu}_A | \Phi_{\text{rv}}^{(\text{i})} \rangle$ can be thought of as a unitary transformation of the dipole moment matrix in the representation of primitive functions $|J_{\text{w}} K m_{\text{w}} \tau_{\text{rot}}\rangle |V\rangle$ to the representation of the eigenfunctions $\Phi_{\text{rv}}^{(\text{w})}$ by means of eq 21. Such a transformation involves nested loops and results in N^4 operations, where N is the number of expansion terms in eq 21. It is known that it is more efficient ($\sim N^3$ operations) to perform this transformation in two steps. First, for a given lower state i, the following effective line strength is evaluated

$$S_{\text{i},VK}^A = \langle \Phi_{\text{rv}}^{(\text{i})} | \bar{\mu}_A | \phi_{VK} \rangle \tag{22}$$

where we introduce a short-hand notation ϕ_{VK} for the primitive basis function $|J_{\text{w}} K m_{\text{w}} \tau_{\text{rot}}\rangle |V\rangle$. Once all $S_{\text{i},VK}$ are computed, in the second step, the line strength $S(\text{f} \leftarrow \text{i})$ is evaluated as

$$S(\text{f} \leftarrow \text{i}) = g_{\text{ns}} \sum_{m_{\text{i}},m_{\text{f}}} \sum_{A=X,Y,Z} \left| \sum_{V,K} C_{VK\tau_{\text{rot}}}^{(\text{f})} S_{\text{i},VK}^A \right|^2 \tag{23}$$

The large number of transitions that had to be evaluated was another computational bottleneck. In order to take advantage of our multiprocessor computing facility, we performed the calculation in "batches" involving states with angular momentum quantum numbers J and $J + 1$. This is the smallest grouping that is consistent with the application of the total angular momentum selection rules. The eigenvalue solutions generated for each J were ordered by increasing energy. The program then computed the line strengths for all of the allowed transitions with $J \rightarrow J$ and $J \leftrightarrow J + 1$. The $J + 1 \rightarrow J + 1$ transitions were not computed in order to avoid double counting. This also meant that $\Delta J = J = 0$ transitions, which are not permitted by the selection rules, were not calculated.

4.3. The $J = 0$ Contraction. TROVE[27] uses a variational approach to solve the nuclear Schrödinger equation. It calculates rotation–vibration energies as the eigenvalues of matrix blocks obtained by constructing the matrix representation of the rotation–vibration Hamiltonian in terms of suitable basis functions. The TROVE basis set for $J > 0$ rovibrational calculations employs vibrational eigenfunctions (solutions to the $J = 0$ problem). We call this a $J = 0$ contraction. The vibrational matrix elements of the vibrational parts of the Hamiltonian, which are required for constructing the Hamiltonian matrix at any $J > 0$ are precalculated and stored to disk in order to save memory.

The procedure for constructing the $J = 0$ Hamiltonian is as follows. In the case of NH$_3$, a flexible molecule with a double-well potential surface, the primitive basis functions are formed from the one-dimensional (1D) vibrational functions $\phi_{n_1}(r_1^l)$, $\phi_{n_2}(r_2^l)$, $\phi_{n_3}(r_3^l)$, $\phi_{n_4}(\xi_4^l)$, $\phi_{n_5}(\xi_5^l)$, and $\phi_{n_6}(\bar{\rho})$. Here, n_i are corresponding principal quantum numbers, and the five coordinates $(r_1^l, r_2^l, r_3^l, \xi_4^l, \xi_5^l)$ are linearized versions[24] of the coordinates $(r_1, r_2, r_3, \xi_4, \xi_5)$ introduced in connection with eqs 14–17. The $\phi_{n_i}(\xi)$ functions are generated in numerical solutions to the corresponding 1D Schrödinger equations.[27] In the present TROVE calculations, the Hamiltonians (i.e., both the kinetic energy operator and the potential energy function) are expressed as expansions (of sixth and eighth order, respectively) around the nonrigid reference configuration[48] defined by the "umbrella" coordinate, $\bar{\rho}$. The errors introduced by these truncations have been discussed in detail for H$_2$S and CH$_3^+$ previously.[27] In the present case of NH$_3$, we have checked the convergence of the computed vibrational term values by performing additional calculations where the expansions of the kinetic energy operator and the potential energy functions were extended by two orders (to 8th and 10th order, respectively); the corresponding rms changes in the vibrational term values (see Table 2 below) amount to 0.05 and 0.04 cm^{-1}, respectively.

We could diagonalize the Hamiltonian matrix directly in the representation of the primitive functions ϕ_{n_i}, as described by Yurchenko et al.[27] However, this basis set is not symmetry-adapted, and therefore, it does not factorize the Hamiltonian matrix into smaller symmetry blocks. A more serious problem associated with basis functions that are not symmetry-adapted relates to the intensity simulation, where symmetry plays a crucial role through the nuclear spin statistical weights. Therefore, we prepare from ϕ_{n_i} a set of symmetry-adapted vibrational basis functions ϕ_i^Γ (the details of the symmetrization approach will be reported elsewhere) and diagonalize the vibrational Hamiltonian ($J = 0$) in this basis. Here, $\Gamma = $ A$_1'$, A$_2'$, E$'$, A$_1''$, A$_2''$, and E$''$. The resulting eigenfunctions $\Psi_{J=0,\text{i}}^\Gamma$ are then multiplied by the rotational factor $|J,K,m,\tau_{\text{rot}}\rangle$ and then symmetrized again, which results in our final basis functions $\Psi_{J,K,\text{i}}^\Gamma$. These form the $J = 0$ contracted basis set mentioned above.

It is reasonable to assume that our $J = 0$ representation will reduce the nondiagonal elements of the Hamiltonian matrix, making the $J = 0$ contracted basis set more compact than the primitive basis functions from which it is constructed and hence simplifying the calculation of the Hamiltonian matrix.

The Hamiltonian operator can be written in the following general form[27]

$$H = H_{vib} + \frac{1}{2}\sum_{\alpha\beta} J_\alpha G_{\alpha\beta} J_\beta + \frac{1}{2}\sum_{\alpha\lambda}(p_\lambda G_{\lambda\alpha} + G_{\lambda\alpha}p_\lambda)J_\alpha \tag{24}$$

where J_α ($\alpha = x, y, z$) and p_λ are the rotational and vibrational momentum operators, respectively, and H_{vib} is a pure vibrational ($J = 0$) Hamiltonian

$$H_{vib} = \frac{1}{2}\sum_{\lambda\mu} p_\lambda G_{\lambda\mu} p_\mu + V + U \tag{25}$$

used in computing the $J = 0$ eigenfunctions. $G_{\alpha\beta}$, $G_{\lambda\alpha}$, and $G_{\lambda\mu}$ are the kinetic energy factors, U is the pseudopotential,[27] and V is the molecular potential energy function. The vibrational part H_{vib} is diagonal in our $J = 0$ basis set functions $\Psi^\Gamma_{J=0,i}$

$$\langle \Psi^\Gamma_{J=0,i}|H_{vib}|\Psi^\Gamma_{J=0,i'}\rangle = E^{vib}_i \delta_{i,i'} \tag{26}$$

and thus its matrix elements do not need to be calculated. The evaluation of the Hamiltonian matrix can be further simplified by precomputing the matrix elements of all vibrational parts in eq 24

$$G^{\Gamma,\Gamma',i,i'}_{\alpha,\beta} = \langle \Psi^\Gamma_{J=0,i}|G_{\alpha,\beta}|\Psi^{\Gamma'}_{J=0,i'}\rangle \tag{27}$$

$$G^{\Gamma,\Gamma',i,i'}_{\lambda,\alpha} = \langle \Psi^\Gamma_{J=0,i}|p_\lambda G_{\lambda\alpha} + G_{\lambda\alpha}p_\lambda|\Psi^{\Gamma'}_{J=0,i'}\rangle \tag{28}$$

The left-hand side of these equations is given in the representation of the $J = 0$ contracted functions, while the right-hand side is computed in terms of the primitive basis functions ϕ^Γ_k, which appear in the variational expansions of $\Psi^\Gamma_{J=0,i}$. All terms with contribution from the expansion coefficient of less than 10^{-16} are excluded. This speeds up the computation of $G^{\Gamma,\Gamma',i,i'}_{\alpha,\beta}$ and $G^{\Gamma,\Gamma',i,i'}_{\lambda\alpha}$. Equations 27 and 28 represent the last stage where the bulky primitive basis set is utilized. The rest of the computation is performed in terms of the contracted basis functions $\Psi^\Gamma_{J,K,i}$. These are used to evaluate the Hamiltonian matrix for all nonzero values of J. The following equation illustrates the process

$$\langle \Psi^\Gamma_{J,K,i}|H|\Psi^\Gamma_{J,K',i'}\rangle = E^{vib}_i \delta_{i,i'}\delta_{K,K'} + $$
$$\frac{1}{2}\sum_{\tau'_{rot},\tau''_{rot},\Gamma',\Gamma''}\sum_{\alpha\beta}\langle JKm\tau'_{rot}|J_\alpha J_\beta|JK'm\tau''_{rot}\rangle \otimes G^{\Gamma',\Gamma'',i,i'}_{\alpha,\beta} + $$
$$\frac{1}{2}\sum_{\tau'_{rot},\tau''_{rot},\Gamma',\Gamma''}\sum_{\lambda,\alpha}\langle JKm\tau'_{rot}|J_\alpha|JK'm\tau''_{rot}\rangle \otimes G^{\Gamma,\Gamma',i,i'}_{\lambda,\alpha} \tag{29}$$

where the sign $\otimes$ represents the reduction of the product $\Psi^\Gamma_{J=0,i}|J,K,\tau_{rot}\rangle$ to the irreducible representation $\Psi^\Gamma_{J,K,n}$. The computation of the matrix elements of H according to eq 29 in the $J = 0$ representation becomes very quick. Utilizing

"diagonal" vibrational basis functions is in the spirit of the efficient discrete variable representation (DVR) applied in conjunction with the Gauss–Legendre technique.[49]

Along with the matrix elements $G^{\Gamma,\Gamma',i,i'}_{\alpha,\beta}$ and $G^{\Gamma,\Gamma',i,i'}_{\lambda,\alpha}$, we also compute the $J = 0$ contracted matrix elements of the dipole moment components $\bar\mu_\alpha$ appearing in eq 10. This simplifies the calculations of line strength (eq 19). We also utilize the fact that the matrix elements $\langle \Psi^\Gamma_{J,K,i}|H|\Psi^\Gamma_{J,K',i'}\rangle$ are nonzero only for $|K - K'| \leq 2$, and the Hamiltonian matrix can thus be arranged as a rectangular array, thereby reducing memory requirements, particularly in the case of high J values.

The routine selected for diagonalization depends on the size of the matrix. For less-demanding applications, we use the LAPACK[40] routine DSYEVR, which is fast and accepts restrictions for the eigenvalues to be found. For large matrices ($J > 12$ rovibrational calculations), we choose the iterative diagonalizer DSAUPD from the ARPACK package.[50]

5. Results

5.1. Refinement of the Potential Energy Surface. For the present study, we start from a published "spectroscopic" PES (referred to as PES-1) of NH_3.[19] This PES-1 surface was obtained by refining the CBS**-5 potential parameters of an ab initio CCSD(T)/CBS surface through least-squares fittings to the experimental vibrational band centers below 6100 cm^{-1} available in the literature.[19] The analytic form of PES-1 contains the ab initio AQZfc values of the equilibrium constants r_e and α_e of NH_3. Here, as a further refinement, we also optimize these equilibrium constants to improve the description of the interband rotational energy distribution. Toward this end, we first tested the following three choices: (I) the AQZfc ab initio values $r_e = 1.010313$ Å and $\alpha_e = 106.723°$;[19] (II) the most recent spectroscopic values of Huang et al.,[20] $r_e = 1.0107$ Å and $\alpha_e = 106.75°$; and (III) the semiempirical values $r_e = 1.01139$ Å and $\alpha_e = 107.17°$ obtained from a combination of theory and experiment.[51] The variationally computed rotational energies $E_{J,v=0}$ of NH_3 ($J \leq 5$) corresponding to (I), (II), and (III) are listed in Table 1, where we compare them to experimental rotational term values of NH_3.[52] The results for (II)[20] are close to the experiment. We further optimized the equilibrium constants (using the ab initio values (I) as starting parameters) through a nonlinear fit to the experimental values for $J \leq 5$ given in Table 1. One iteration was enough to reduce the rms deviation to 0.0020 cm^{-1} (see the last column of Table 1), with the equilibrium constants $r_e = 1.010772$ Å and $\alpha_e = 106.730°$, which further improve on the values (II).[20] The improvements by this adjustment are significant and reflect the decisive influence of the equilibrium constants on the molecular rotational spectrum. The results of the fit for PES-1 will depend on the approximations made in the TROVE calculations during the refinement; tests with different truncations for the kinetic energy operator, the potential energy function, and the vibrational basis set indicate that the corresponding uncertainties in the adjusted equilibrium bond length and angle are less than 10^{-5} Å and 0.001°, respectively.

We thus adopt these optimized values of the equilibrium constants. All results presented in the remainder of this article are based on the analytical potential energy function which contains the optimized potential parameters from PES-1[19] and the adjusted equilibrium constants (see above). This PES will be referred to as PES-2. We note that PES-1 is given as part of the Supporting Information of Yurchenko et al.,[19] and PES-2 is obtained from PES-1 by substituting the new equilibrium parameters given in footnote d of Table 1.

TABLE 1: Theoretical Rotational Term Values ($J \le 5$) of NH$_3$ Computed with TROVE Using Different Equilibrium Structure Constants

states			term values (cm^{-1})				
J	K	τ_{rot}	obs.	obs.-I[a]	obs.-II[b]	obs.-III[c]	obs.-IV[d]
1	1	0	16.1730	−0.0158	−0.0022	0.0245	−0.0001
1	0	1	19.8899	−0.0190	−0.0060	−0.0423	−0.0002
2	2	0	44.7960	−0.0443	−0.0027	0.1404	−0.0003
2	1	0	55.9387	−0.0539	−0.0142	−0.0600	−0.0006
3	3	0	85.8616	−0.0854	−0.0016	0.3474	−0.0006
3	2	0	104.4221	−0.1015	−0.0208	0.0136	−0.0010
3	1	0	115.5366	−0.1111	−0.0322	−0.1861	−0.0013
3	0	1	119.2379	−0.1144	−0.0360	−0.2526	−0.0014
4	4	0	139.3581	−0.1391	0.0012	0.6454	−0.0008
4	3	0	165.3311	−0.1618	−0.0257	0.1781	−0.0016
4	2	0	183.8291	−0.1781	−0.0448	−0.1543	−0.0021
4	1	0	194.9063	−0.1878	−0.0562	−0.3533	−0.0024
5	5	0	205.2692	−0.2053	0.0057	1.0341	−0.0010
5	4	0	238.6527	−0.2348	−0.0291	0.4331	−0.0022
5	3	0	264.5166	−0.2579	−0.0559	−0.0317	−0.0030
5	2	0	282.9372	−0.2744	−0.0749	−0.3625	−0.0035
5	1	0	293.9683	−0.2843	−0.0862	−0.5604	−0.0038
5	0	1	297.6418	−0.2876	−0.0900	−0.6263	−0.0039

[a] PES-1: Using $r_e = 1.010313$ Å and $\alpha_e = 106.723°$.[19] [b] Obtained using $r_e = 1.0107$ Å and $\alpha_e = 106.75°$.[20] [c] Obtained using $r_e = 1.01139$ Å and $\alpha_e = 107.17°$.[51] [d] PES-2: Obtained using $r_e = 1.010772$ Å and $\alpha_e = 106.730°$ (this work).

To illustrate the effect of this refinement, we show part of the rotational spectrum of NH$_3$ as a "stick" diagram on the left panel of Figure 1. The upper half represents the experimental lines as collected in the HITRAN 2004 database,[12] while the lower half gives the theoretical transitions computed with the TROVE approach. Lines computed with the refined equilibrium structure (PES-2, solid sticks) show excellent agreement with experiment, while the lines obtained utilizing the ab initio values (PES-1, dashed sticks) are skewed toward larger wavenumbers.

5.2. Basis Set Convergence and Empirical Adjustment of the Vibrational Band Centers. The size of the Hamiltonian matrix is an important factor that influences the accuracy with which high rovibrational states can be computed, and consequently, it is important to derive by empirical methods the smallest basis set that is consistent with the required eigenvalue accuracy (that is to say, the optimum size for "convergence").

TROVE employs polyad number truncation[24,27] to control the size of the vibrational basis set, with the polyad number P given by

$$P = 2(n_1 + n_2 + n_3) + n_4 + n_5 + \frac{n_6}{2} \qquad (30)$$

where n_i are the quantum numbers connected with the primitive functions ϕ_{n_i}. That is, we include in the primitive basis set only those functions ϕ_n for which $P \le P_{max}$. We find that in order to achieve convergence to within 0.1 cm^{-1}, P_{max} must be in the range of 14–16.

A full rovibrational calculation with truncation at $P_{max} = 16$ is very expensive, and it is thus desirable to devise a procedure where these calculations can be done with a smaller basis set (e.g., truncated at $P_{max} = 12$) without much loss of accuracy. We recall that the vibrational part of the Hamiltonian is diagonal in the $J = 0$ basis set and that the Hamiltonian matrix in eq 29 is formed using the vibrational energies E_i^{vib} obtained as eigensolutions of eq 26. When constructing the full Hamiltonian matrix in a given basis, we can thus substitute these energies

with more converged values E_i^{vib} that have been precomputed using a larger $J = 0$ basis with a higher P_{max} value. More specifically, we compute the rotational part of the Hamiltonian matrix in eq 29 using the small $P_{max} = 12$ basis set $\Psi_{J,K,n}^\Gamma$, while the vibrational part (given by the diagonal terms E_i^{vib}) is evaluated with the large $P_{max} = 16$ vibrational basis set. This procedure leads to reasonable convergence, that is, to results very close to those from the full $P_{max} = 16$ treatment. The reason why this approach works well is related to the separation between the vibrational and rotational degrees of freedom achieved through the $J = 0$ contraction. The vibrational motion is most difficult to converge, and this can only be achieved by using the extended $P_{max} = 16$ vibrational basis set. The Coriolis interaction is less demanding because of the use of the Eckart–Sayvetz coordinate system[27,53,54] in TROVE, and the required degree of accuracy can thus be reached with the much smaller $P_{max} = 12$ basis set in the rotational part.

The vibrational term values could be converged even more tightly by extrapolating the $P_{max} = 12$, 14, and 16 values of E_i^{vib} to the complete vibrational basis set limit.[55] However, this is not considered necessary for the purpose of generating a line list since the corrections from such an extrapolation will be small compared with the inherent errors in the term values that are caused by the imperfection of the underlying potential energy surface. Instead, if we aim for higher accuracy in a pragmatic manner, we can resort to a more empirical approach where the theoretical E_i^{vib} term values in eq 29 are replaced by accurate experimental term values, $E_{J=0,i}^{exp}$, whenever these are available in the published literature. In this case, we adjust the vibrational band centers "by hand", and by doing so, we shift the rotational energy structure toward better agreement with experiment. This procedure can be regarded as an empirical basis set correction scheme and will be denoted as the EBSC scheme.

Table 2 lists the vibrational band centers of ammonia up to 7000 cm^{-1}, as derived from experimental data and from variational calculations ($J = 0$). On the theoretical side, we quote the recent results of Huang et al.,[20] which are based on a high-level coupled cluster potential energy surface (with various corrections) that has been carefully refined against the most reliable $J = 0$–2 transitions in the HITRAN 2004 database below 5300 cm^{-1}. These results[20] are in excellent agreement with experiment (rms error of 0.023 cm^{-1} for 13 HITRAN 2004 bands below $J = 2$). The corresponding analytical potential function (with 3393 parameters) is not available to us and can thus not be used for TROVE calculations.

Our own previous refinement[19] that led to the PES-1 surface (see above) yielded rms errors of 0.4 (3.0) cm^{-1} for the vibrational band centers below 6100 (10300) cm^{-1} in variational XY3 calculations where the kinetic energy and potential energy expansions were truncated at sixth order. In the present work, we truncate the potential energy expansions at eighth order and use the PES-2 surface (see above). Both of these changes will have the effect of "detuning" the previous refinement.[19] This can be seen in the last two columns of Table 2, which list the current TROVE results for PES-2 using $P_{max} = 12$ and 16. The deviations from experiment are usually in the range of 0–3 cm^{-1}, and the rms errors amount to 1.8 and 2.4 cm^{-1}, respectively (for term values below 6100 cm^{-1} excluding those at 3462 and 4055 cm^{-1}, which are not precisely known, see Yurchenko et al.).[19] To achieve higher accuracy for the vibrational band centers, another more thorough refinement of our PES would be needed, similar in spirit to that of Huang et al.[20] A pragmatic alternative is the EBSC scheme outlined above, which, by construction, will give exact agreement with the
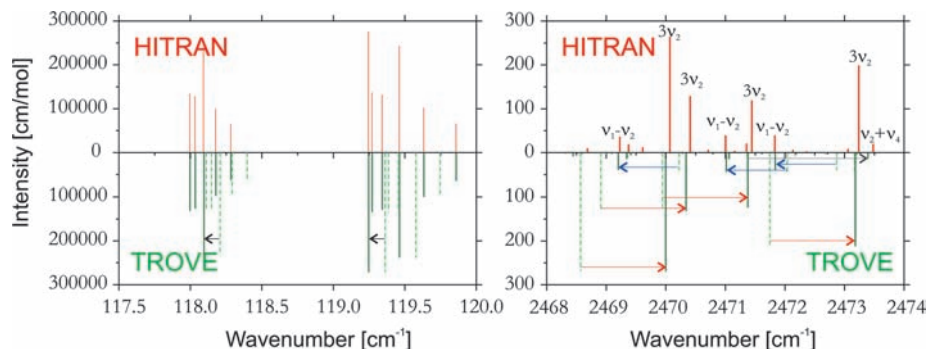
Figure 1. Comparison of the simulated and observed (HITRAN) spectra of the rotational (left panel) and the $3\nu_2/\nu_2 + \nu_4/\nu_1 - \nu_2$ band system (right panel) represented as stick diagrams. The lower plots show the effect of the empirical adjustments of the equilibrium constants (left panel) and the band centers (right panel, EBSC scheme) as a shift from the dashed to solid lines (see text).

TABLE 2: Vibrational Band Centers (cm^{-1}) of ^{14}NH$_3$ Derived from Experimental Data and from Variational Calculations

Γ	state	ref.	obs.^{a}	Huang et al.^{b20}	$P_{\max} = 12^c$	$P_{\max} = 16^d$
A'	ν_2^+	52	932.43^e	932.38	931.67	931.64
	$2\nu_2^+$	67	1597.47^e	1597.44	1595.94	1595.88
	$3\nu_2^+$	68	2384.15^e	1597.44	2382.71	2382.63
	$2\nu_4^{0,+}$	69	3216.10^e	3215.90	3213.90	3213.52
	ν_1^+	69	3336.11^e	3336.09	3335.63	3335.60
	$4\nu_2^+$	70	3462.00	3462.26	3461.10	3461.00
	$(\nu_2 + 2\nu_4^0)^+$	71	4115.62^e	4115.83	4112.50	4110.94
	$(\nu_1 + \nu_2)^+$	71	4294.53^e	4294.48	4293.46	4293.32
	$(\nu_1 + 2\nu_4)^+$	72	6520.00	6519.78	6516.34	6515.16
	$2\nu_1^+$	72	6606.00	6605.03	6600.89	6600.40
	$2\nu_3^+$	65	6795.96	6797.38	6794.60	6794.24
E'	ν_4^+	12	1626.27^e	1626.25	1625.09	1625.02
	$(\nu_2 + \nu_4)^+$	69	2540.53^e	2540.49	2538.50	2538.29
	$2\nu_4^{\pm2,+}$	12	3240.16^e	3240.14	3237.71	3237.44
	ν_3^+	12	3443.68^e	3443.60	3443.94	3443.90
	$(\nu_2 + 2\nu_4^{\pm2})^+$	71	4135.94^e	4136.09	4132.67	4131.56
	$(\nu_2 + \nu_3)^+$	12	4416.92^e	4416.90	4416.40	4416.23
	$(\nu_1 + \nu_4)^+$	12	4955.76^e	4955.70	4953.56	4953.26
	$(\nu_3 + \nu_4)^+$	12	5052.63^e	5052.59	5051.59	5051.21
	$(\nu_2 + \nu_3 + \nu_4)^+$	72	6012.90^e	6012.73	6009.52	6008.64
	$(\nu_1 + 2\nu_4^{\pm2})^+$	66	6556.42^e	6556.50	6552.20	6551.18
	$(\nu_1 + \nu_3)^+$	66	6608.15	6609.73	6605.36	6604.32
	$(\nu_3 + 2\nu_4^2)^+$	63	6678.36	6678.48	6670.05	6669.47
	$2\nu_3^+$	72	6850.20	6850.25	6850.17	6849.94
A''	0^-	12	0.79^e	0.80	0.81	0.80
	ν_2^-	73	968.12^e	968.12	967.48	967.45
	$2\nu_2^-$	67	1882.18^e	1882.14	1880.99	1880.91
	$3\nu_2^-$	68	2895.52^e	2895.44	2894.11	2894.00
	$2\nu_4^{0,-}$	12	3217.58^e	3217.53	3216.00	3215.27
	ν_1^-	69	3337.11^e	3337.07	3335.63	3336.66
	$4\nu_2^-$	74	4055.00	4061.40	4060.46	4060.22
	$(\nu_1 + 2\nu_4^0)^-$	71	4173.25^e	4173.13	4171.18	4169.58
	$(\nu_1 + \nu_2)^-$	12	4320.04^e	4319.97	4319.16	4318.98
	$2\nu_3^{0,-}$	65	6795.46	6795.96	6793.42	6792.84
E''	ν_4^-	12	1627.37^e	1627.35	1626.23	1626.13
	$(\nu_2 + \nu_4)^-$	12	2586.13^e	2586.09	2584.45	2584.14
	$2\nu_4^{\pm 2,-}$	69	3241.62^e	3241.57	3239.53	3238.98
	ν_3^-	12	3443.98^e	3443.96	3444.36	3444.26
	$(\nu_2 + 2\nu_4^{\pm2})^-$	71	4193.14^e	4193.14	4190.60	4189.45
	$(\nu_2 + \nu_3)^-$	71	4435.45^e	4435.41	4435.12	4434.90
	$(\nu_1 + \nu_4)^-$	12	4956.91^e	4956.85	4954.94	4954.53
	$(\nu_3 + \nu_4)^-$	72	5053.24^e	5053.19	5052.32	5051.82
	$(\nu_2 + \nu_3 + \nu_4)^-$	72	6037.12^e	6036.33	6034.50	6032.98
	$(\nu_1 + 2\nu_4^2)^-$	66	6557.93^e	6558.17	6554.94	6552.94
	$(\nu_1 + \nu_3)^-$	66	6609.72	6610.66	6607.78	6605.61
	$(\nu_3 + 2\nu_4^2)^-$	63	6679.15^e	6679.17	6671.62	6670.38
	$2\nu_3^-$	72	6850.70^e	6850.65	6850.93	6850.38

^{a} Derived from experimental data. ^{b} $J = 0$ band centers of Huang et al.[20] computed using their refined PES. ^{c} Computed using the $P_{\max} = 12$ basis set in conjunction with PES-2. ^{d} Computed using the $P_{\max} = 16$ basis set in conjunction with PES-2. ^{e} Experimental values of band centers $E_{J=0,i}^{\exp}$ used in the present EBSC scheme (see text).

available experimental band centers in $J = 0$ calculations. When generating a line list using the EBSC scheme, the imperfection of the chosen PES will thus enter only through the computed band centers of bands where reliable experimental data are

missing and through the rovibrational couplings that affect the full rovibrational calculations. Another source of error is the limited accuracy of the available experimental data, for example, in the HITRAN database, and care must be exercised in selecting only reliable such data.[20]

For the remainder of this paper, we adopt the EBSC scheme in combination with PES-2. The vibrational term values used in this scheme are marked in Table 2; 37 of them are taken from experiment, and the 4401 remaining ones from the $P_{\max} = 16$ calculations. The incorporation of experimental information in the EBSC scheme is obviously a departure from a purely ab initio approach, which is considered to be justified by the gain in accuracy that can be achieved when computing an extensive rovibrational line list.

As an illustration, we show in Figure 1 (right panel) a part of the simulated cool spectrum of ammonia (stick diagram) for a number of selected transitions from the band system $3\nu_2/2\nu_4/\nu_1 - \nu_2$. As before, the upper panel (HITRAN) visualizes the experimental data. The lower panel represents the $P_{\max} = 12$ (dashed lines) and EBSC (solid lines) transitions, that is, spectra computed without and with the empirical adjustment of E_i^{vib} to the experimental values. All three bands that appear in the given frequency window experience different shifts of their centers such that the deviations between the HITRAN and EBSC lines drop from typically 1–2 to less than 0.1 cm^{-1}. Of course, the solid lines from the top and bottom parts should ideally coincide; the remaining slight misalignment between them is due to the limitations of the EBSC scheme that have been outlined above.

5.3. Vibrational Transition Moments. The vibrational transition moments are defined as

$$\mu_{\mathrm{fi}} = \sqrt{\sum_{\alpha=x,y,z} \left| \langle \Psi_{J=0,\mathrm{f}}^{\Gamma} | \bar{\mu}_{\alpha} | \Psi_{J=0,\mathrm{i}}^{\Gamma} \rangle \right|^2} \qquad (31)$$

in terms of the vibrational wave functions $\Psi_{J=0,\mathrm{w}}^{\Gamma}$, w = i or f, and the dipole components $\bar{\mu}_{\alpha}$ oriented along the Eckart axes.[61] For calculating the vibrational wave functions, we use the EBSC scheme with the PES-2 surface and the basis set truncated at polyad number $P_{\max} = 12$. The electronically averaged dipole moment functions $\bar{\mu}_{\alpha}$ in eq 31 are derived from the AQZfc ab initio dipole moment surface by solving the linear system eq 10 as discussed above. We have computed the transition moments in eq 31 for all vibrational transitions that are relevant for the $T = 300$ K absorption spectrum. In Table 3, we list a number of selected transition moments for which experimental information is available in the literature.[42,56–60] The agreement with experiment is good.

A Variationally Computed $T = 300$ K Line List for NH$_3$

J. Phys. Chem. A, Vol. 113, No. 43, 2009 **11853**

TABLE 3: Band Centers ν_{fi} and Vibrational Transition Moments μ_{fi} for NH$_3$; Transitions Originating in the Vibrational Ground State

| states		ν_{fi}/cm^{-1}		μ_{fi}/D		
f	i	obs.[a]	obs.[b]	ref.[c]	ATZfc[d]	AQZfc[e]
0^-	0^+	0.79	1.47193(1)	45	1.4564	1.4638
ν_2^+	0^-	931.64	0.248(7)	75	0.2445	0.2467
ν_2^-	0^+	968.12	0.236(4)	75	0.2347	0.2366
$2\nu_2^+$	0^-	1596.68	0.02036(25)	67	0.0202	0.0210
ν_4^+	0^+	1626.27	0.08408(34)	67	0.0828	0.0841
ν_4^-	0^-	1626.58	0.08408(34)	67	0.0827	0.0840
$2\nu_2^-$	0^+	1882.18	0.003256(35)	67	0.0026	0.0030
$3\nu_2^+$	0^-	2383.35	0.00496(13)	68	0.0054	0.0053
$(\nu_2 + \nu_4)^+$	0^+	2540.53	0.002358(36)	68	0.0091	0.0085
$(\nu_2 + \nu_4)^-$	0^-	2894.73	0.002182(82)	68	0.0094	0.0089
$3\nu_2^-$	0^+	2895.52	0.002856(40)	68	0.0027	0.0027
$2\nu_4^{0,+}$	0^-	3215.31	0.00920(6)[f]	70	0.0073	0.0064
$2\nu_4^{0,-}$	0^+	3217.58	0.00920(6)[f]	70	0.0074	0.0066
$2\nu_4^{\pm2,+}$	0^+	3240.16	0.00920(6)[f]	70	0.0091	0.0089
$2\nu_4^{\pm2,-}$	0^+	3240.82	0.00920(6)[f]	70	0.0090	0.0088
ν_1^+	0^-	3335.31	0.0262(1)	70	0.0269	0.0260
ν_1^-	0^+	3337.11	0.0262(1)	70	0.0270	0.0261
ν_3^-	0^-	3443.19	0.0182(1)	70	0.0180	0.0201
ν_3^+	0^+	3443.63	0.0182(1)	70	0.0181	0.0202
$(\nu_1 + \nu_2)^+$	0^-	4293.74	0.0079	76	0.0087	0.0088
$(\nu_1 + \nu_2)^-$	0^+	4320.04	0.0079	76	0.0083	0.0084
$(\nu_2 + \nu_3)^+$	0^+	4416.92	0.0206	76	0.0246	0.0250
$(\nu_2 + \nu_3)^-$	0^-	4434.65	0.0206	76	0.0244	0.0248

[a] Experimental data taken from Table 2. [b] Experimental uncertainties given in parentheses, in units of the last digit quoted. [c] Reference for the experimental transition moment value. [d] Taken from Yurchenko et al.,[19] XY3 calculation, PES CBS**5, ATZfc DMS. [e] Present work, TROVE calculation, EBSC scheme, PES-2, AQZfc DMS. [f] The experimental value corresponds to the total $2\nu_4^{\pm}$ transition moment and can thus not be directly compared to the separate theoretical values for $2\nu_4^{0,\pm}$ and $2\nu_4^{\pm2,\pm}$, respectively.

The present AQZfc theoretical values are found to be very similar to the previous ATZfc results[22] (also listed in Table 3) obtained using the XY3 approach.[24] The upgrade of the ab initio dipole moment surface from CCSD(T)/aug-cc-pVTZ to CCSD(T)/aug-cc-pVQZ does not significantly affect the values of μ_{fi}, which implies that the ab initio DMS is essentially converged at this level. The complete list of theoretical transition moments is given as Supporting Information.

5.4. Intensity Simulations. In order to simulate absorption spectra at a given T and within a particular wavenumber range, the upper and lower energies and the Einstein coefficients $A(f \leftarrow i)$ (or the line strengths) of all transitions in this range must be known; in practice, only the transitions above a certain minimum intensity are included. The simplest way to present the spectral data is a stick diagram where the height gives the integrated absorption coefficient from eq 20. In this section, we report such simulations for the NH$_3$ absorption bands covering the frequency range of 0–8000 cm^{-1}. The line strengths entering eq 20 are computed from eq 19 with the spin statistical weights g_{ns} from Table 2 of Yurchenko et al.[21] The simulations are carried out using the PES-2 surface and the AQZfc DMS. We used a value of 1762 for the partition function, Q, at 300 K, which was obtained by summing over all variational term values below 8000 cm^{-1}. With the limits defined above, we computed 4 943 196 transitions, of which we selected 3 249 988 with intensities >10^{-4} cm mol^{-1}.

Figure 2 shows the simulated ($T = 300$ K) absorption spectrum (TROVE) and experimental (HITRAN) absorption spectrum of NH$_3$ for the whole simulation range. The logarithmic scale allows almost all transitions to be displayed and
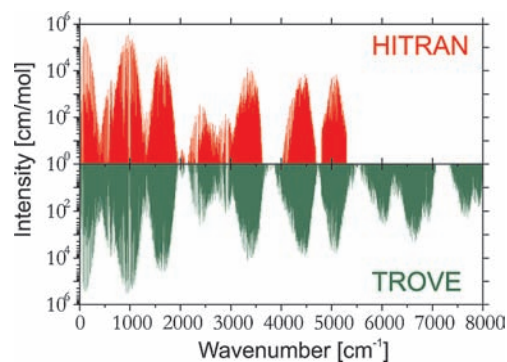
Figure 2. Overview of the simulated absorption ($T = 300$ K) spectrum (TROVE) of NH$_3$ compared to experiment (HITRAN).

reveals the gaps and limitations of the HITRAN 2004 database. Our intensities based on the ab initio DMS are in very good qualitative agreement with experiment. This can be better appreciated in Figure 3, where the first six band systems (0–300, 700–1200, 1400–1900, 2200–2800, 3100–3600, and 4150–4650 cm^{-1}) are shown in more detail. The largest deviation from the HITRAN 2004 intensities are observed around 4400 cm^{-1}. In general, the computed and experimental (HITRAN) rotational band intensities agree very well (see Figures 1 and 3). However, we hope that the accuracy of our theoretical spectrum will enable experimentalists to assign so-far unidentified transitions in these and other regions. It should also be noted that the region around 1.5 μm (near 6500 cm^{-1}) that is not covered in HITRAN 2004 has been the subject of a number of recent experimental studies.[62–66]

Figure 4 takes a closer look at the simulated spectrum by comparing the theoretical intensities with the available experimental data[12] in two selected wavenumber windows, 1622–1632 ($2\nu_2/\nu_4$ system) and 3333–3337 cm^{-1} ($\nu_1/4\nu_2/\nu_3/2\nu_4$ system). Not all of the experimentally known band centers have been accurately determined, and many are unknown. This is the largest source of error in our simulations with the EBSC scheme, which employs theoretical vibrational band centers in such cases (see above). The accuracy of these theoretical values for the PES-2 surface may generally not be sufficient to properly position the closely lying dark states and to capture their effects on the rovibrational structure.

As a further illustration of the quality of our simulations, we show in Figure 5 a synthetic spectrum convolved with a Gaussian profile (HWHM = 0.01 cm^{-1}) together with the observed spectrum (Kitt peak data) of NH$_3$ at 0.35 Torr and 295 K. It is obvious that the two spectra match very well.

Our complete cool NH$_3$ line list is given as Supporting Information. It details the transition energies, line strengths, and Einstein coefficients $A(f \leftarrow i)$ and also includes the absorption intensities estimated for $T = 300$ K. A Fortran program is provided to generate synthetic spectra using this line list at other specified temperatures. However, such spectra will become increasingly inaccurate as the temperature is increased.

6. Conclusion

We have presented calculated spectra for ammonia covering a large part of the infrared region. Detailed comparisons with observed room-temperature spectra show excellent agreement for the position and intensity of the transitions. These comparisons also indicate that the HITRAN database[12] is rather incomplete in its coverage of the infrared spectrum of ammonia. A number of other problems concerning the HITRAN data for
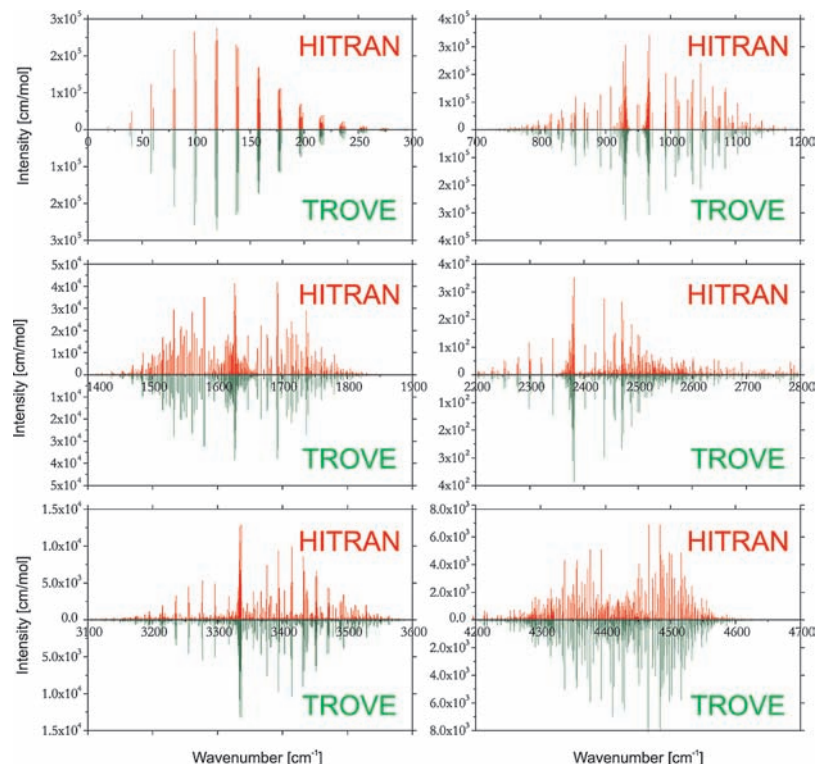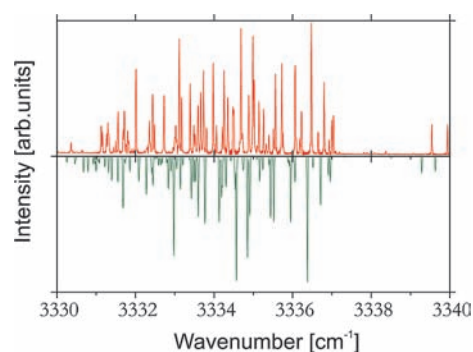
Figure 3. Comparison of the simulated (TROVE) and observed (HITRAN) spectra of NH_3 at $T = 300$ K for several low-lying band systems.
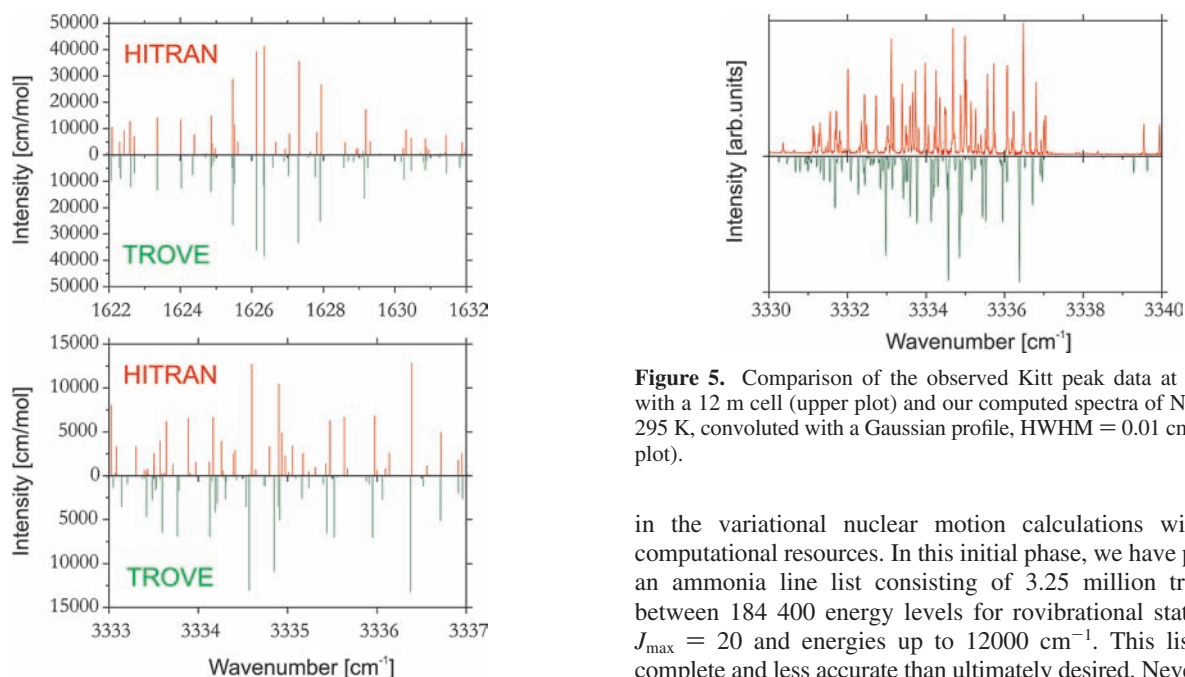
Figure 4. Comparison of the simulated (TROVE) and observed (HITRAN) spectra of NH_3 at $T = 300$ K in two selected frequency regions.

Figure 5. Comparison of the observed Kitt peak data at 0.35 Torr with a 12 m cell (upper plot) and our computed spectra of NH_3 at $T = 295$ K, convoluted with a Gaussian profile, HWHM $= 0.01$ cm^{-1} (lower plot).

in the variational nuclear motion calculations within our computational resources. In this initial phase, we have produced an ammonia line list consisting of 3.25 million transitions between 184 400 energy levels for rovibrational states up to $J_{max} = 20$ and energies up to 12000 cm^{-1}. This list is less complete and less accurate than ultimately desired. Nevertheless, it can be used to produce synthetic NH_3 spectra that agree well with observation at room temperature.

Supporting Information Available: The parameters $\mu_{k,l,m,\ldots}^{(\Gamma)}$ (see eqs 11−13) together with the Fortran routine for calculating the dipole moment components; the complete cool NH_3 line list with transition energies, line strengths, and Einstein coef-

ammonia were identified in the course of this work and will be discussed elsewhere.

Our ultimate aim is the construction of an NH_3 line list capable of replicating observed spectra at temperatures up to ~1500 K. Inter alia, this will enable a better understanding of the atmospheric signatures of brown dwarfs and exoplanets. The work presented here represents the first step toward this goal, which involves the generation, refinement, and validation of the required potential energy and dipole moment surfaces, as well as establishment of the level of accuracy that can be achieved

ficients $A(f \leftarrow i)$, as well as absorption intensities estimated for $T = 300$ K; and a Fortran program to generate synthetic spectra. For this material, see http://www.tampa.phys.ucl.ac.uk/ftp/astrodata/NH3/. This material is available free of charge via the Internet at http://pubs.acs.org.

References and Notes

(1) Kawakita, H.; Watanabe, J.-I. *Astrophys. J.* **2002**, *572*, L177.
(2) Lara, L.-M.; Bézard, B.; Griffith, C. A.; Lacy, J. H.; Owen, T. *Icarus* **1998**, *131*, 317.
(3) Fouchet, T.; Lellouch, E.; Bézard, B.; Encrenaz, T.; Drossart, P. *Icarus* **2000**, *143*, 223.
(4) Orton, G.; et al. *Science* **1995**, *267*, 1277.
(5) Kawakita, H.; Dello Russo, N.; Furusho, R.; Fuse, T.; Watanabe, J.-i.; Boice, D. C.; Sadakane, K.; Arimoto, N.; Ohkubo, M.; Ohnishi, T. *Astrophys. J.* **2006**, *643*, 1337.
(6) Kawakita, H.; Jehin, E.; Manfroid, J.; Hutsemékers, D. *Icarus* **2007**, *187*, 272.
(7) Burrows, A.; Marley, M.; Hubbard, W. B.; Lunine, J. I.; Guillot, T.; Saumon, D.; Freedman, R.; Sudarsky, D.; Sharp, C. *Astrophys. J.* **1997**, *491*, 856.
(8) Sharp, C. M.; Burrows, A. *Astrophys. J. Suppl.* **2007**, *168*, 140.
(9) Burrows, A.; Sudarsky, D.; Lenine, J. I. *Astrophys. J.* **2003**, *596*, 587.
(10) Sudarsky, D.; Burrows, A.; Hubeny, I. *Astrophys. J.* **2003**, *588*, 1121.
(11) Swain, M. R.; Vasisht, G.; Tinetti, G. *Nature* **2008**, *452*, 329.
(12) Rothman, L. S.; Jacquemart, D.; Barbe, A.; Benner, D. C.; Birk, M.; Brown, L. R.; Carleer, M. R.; Chackerian, C.; Chance, K.; Coudert, L. H.; Dana, V.; Devi, V. M.; Flaud, J.-M.; Gamache, R. R.; Goldman, A.; Hartmann, J.-M.; Jucks, K. W.; Maki, A. G.; Mandin, J.-Y.; Massie, S. T.; Orphal, J.; Perrin, A.; Rinsland, C. P.; Smith, M. A. H.; Tennyson, J.; Tolchenov, R. N.; Toth, R. A.; Vander, A. J.; Varanasi, P.; Wagner, G. *J. Quant. Spectrosc. Radiat. Transfer* **2005**, *96*, 139.
(13) Martin, J. M. L.; Lee, T. J.; Taylor, P. R. *J. Chem. Phys.* **1992**, *97*, 8361.
(14) Lin, H.; Thiel, W.; Yurchenko, S. N.; Carvajal, M.; Jensen, P. *J. Chem. Phys.* **2002**, *117*, 11265.
(15) Rajamäki, T.; Miani, A.; Pesonen, J.; Halonen, L. *Chem. Phys. Lett.* **2002**, *36*, 226.
(16) Rajamäki, T.; Miani, A.; Halonen, L. *J. Chem. Phys.* **2003**, *118*, 6358.
(17) Rajamäki, T.; Miani, A.; Halonen, L. *J. Chem. Phys.* **2003**, *118*, 10929.
(18) Rajamäki, T.; Kállay, M.; Noga, J.; Valiron, P.; Halonen, L. *Mol. Phys.* **2004**, *102*, 2297.
(19) Yurchenko, S. N.; Zheng, J.; Lin, H.; Jensen, P.; Thiel, W. *J. Chem. Phys.* **2005**, *123*, 134308.
(20) Huang, X.; Schwenke, D. W.; Lee, T. J. *J. Chem. Phys.* **2008**, *129*, 214304.
(21) Yurchenko, S. N.; Thiel, W.; Carvajal, M.; Lin, H.; Jensen, P. *Adv. Quantum Chem.* **2005**, *48*, 209.
(22) Yurchenko, S. N.; Carvajal, M.; Lin, H.; Zheng, J.; Thiel, W.; Jensen, P. *J. Chem. Phys.* **2005**, *122*, 104317.
(23) Mátyus, E.; Czakó, G.; Császár, A. G. *J. Chem. Phys.* **2009**, *130*, 134112.
(24) Yurchenko, S. N.; Carvajal, M.; Jensen, P.; Lin, H.; Zheng, J.; Thiel, W. *Mol. Phys.* **2005**, *103*, 359.
(25) Yurchenko, S. N.; Carvajal, M.; Thiel, W.; Jensen, P. *J. Mol. Spectrosc.* **2006**, *239*, 71.
(26) Yurchenko, S. N.; Thiel, W.; Carvajal, M.; Jensen, P. *Chem. Phys.* **2008**, *346*, 146.
(27) Yurchenko, S. N.; Thiel, W.; Jensen, P. *J. Mol. Spectrosc.* **2007**, *245*, 126.
(28) Herzberg, G. *Infrared and Raman Spectra of Polyatomic Molecules*; D. Van Nostrand Co. Inc.: New York, 1945.
(29) Bunker, P. R.; Jensen, P. *Molecular Symmetry and Spectroscopy*, 2nd ed.; NRC Research Press: Ottawa, Canada, 1998.
(30) Mills, I. M.; Robiette, A. G. *Mol. Phys.* **1985**, *56*, 743.
(31) Dennison, D. M.; Hardy, J. D. *Phys. Rev.* **1932**, *39*, 938.
(32) Cleeton, C. E.; Williams, N. H. *Phys. Rev.* **1934**, *45*, 234.
(33) Cheung, A. C.; Rank, D. M.; Townes, C. H.; Thornton, D. D.; Welch, W. J. *Phys. Rev. Lett.* **1968**, *21*, 1701.

(34) Werner, H.-J.; Knowles, P. J. *MOLPRO2000*, a package of ab initio programs; with contributions from Amos, R. D.; et al.
(35) (a) Hampel, C,; Peterson, K.; Werner, H.-J. *Chem. Phys. Lett.* **1992**, *190*, 1, and references therein. (b) The program to compute the perturbative triples corrections has been developed by Deegan, M. J. O.; Knowles, P. J. *Chem. Phys. Lett.* **1994**, *227*, 321.
(36) Purvis, G. D.; Bartlett, R. J. *J. Chem. Phys.* **1982**, *76*, 1910.
(37) Raghavachari, K.; Trucks, G. W.; Pople, J. A.; Head-Gordon, M. *Chem. Phys. Lett.* **1989**, *157*, 479.
(38) Dunning, T. H. *J. Chem. Phys.* **1989**, *90*, 1007.
(39) Woon, D. E.; Dunning, T. H. *J. Chem. Phys.* **1993**, *98*, 1358.
(40) Anderson, E.; et al. LAPACK Users' Guide, 3rd ed.; http://www.netlib.org/lapack/ (1999).
(41) Marquardt, R.; Quack, M.; Thanopulos, I.; Luckhaus, D. *J. Chem. Phys.* **2003**, *119*, 10724.
(42) Marshall, M. D.; Izgi, K. C.; Muenter, J. S. *J. Chem. Phys.* **1997**, *107*, 1037.
(43) Halkier, A.; Taylor, P. R. *Chem. Phys. Lett.* **1998**, *285*, 133.
(44) Puzzarini, C. *Theor. Chem. Acc.* **2008**, *121*, 1.
(45) Tanaka, K.; Ito, H.; Tanaka, T. *J. Chem. Phys.* **1987**, *87*, 1557.
(46) Barber, R. J.; Tennyson, J.; Harris, G. J.; Tolchenov, R. N. *Mon. Not. R. Astron. Soc.* **2006**, *368*, 1087.
(47) Bunker, P. R.; Jensen, P. *Fundamentals of Molecular Symmetry*; IOP Publishing: Bristol, U.K., 2004.
(48) Hougen, J. T.; Bunker, P. R.; Johns, J. W. C. *J. Mol. Spectrosc.* **1970**, *34*, 136.
(49) Szalay, V. *J. Chem. Phys.* **1993**, *99*, 1978.
(50) Lehoucq, R. B.; Sorensen, D. C.; Yang, C. *ARPACK Users' Guide: Solution of Large-scale Eigenvalue Problems with Implicitly Restarted Arnoldi Methods (Software, Environments and Tools)*; Society for Industrial & Applied Mathematics: Philadelphia, PA, 1998; http://www.caam.rice.edu/software/ARPACK/.
(51) Pawłowski, F.; et al. *J. Chem. Phys.* **2002**, *116*, 6482.
(52) Chen, P.; Pearson, J. C.; Pickett, H. M.; Matsuura, S.; Blake, G. A. *J. Mol. Spectrosc.* **2006**, *236*, 116.
(53) Eckart, C. *Phys. Rev.* **1935**, *47*, 552.
(54) Sayvetz, A. *J. Chem. Phys.* **1939**, *7*, 383.
(55) Ovsyannikov, R. I.; Thiel, W.; Yurchenko, S. N.; Carvajal, M.; Jensen, P. *J. Chem. Phys.* **2008**, *129*, 044309.
(56) Ueda, Y.; Iwahori, J. *J. Mol. Spectrosc.* **1986**, *116*, 191.
(57) Beckwith, P. H.; Danagher, D. J.; Reid, J. *J. Mol. Spectrosc.* **1987**, *121*, 209.
(58) Cottaz, C.; Tarrago, G.; Kleiner, I.; Brown, L. R. *J. Mol. Spectrosc.* **2001**, *209*, 30.
(59) Takami, M.; Jones, H.; Oka, T. *J. Chem. Phys.* **1979**, *70*, 3557.
(60) Sasada, S.; Hasegawa, Y.; Amano, T.; Shimizu, T. *J. Mol. Spectrosc.* **1982**, *96*, 106.
(61) Le Sueur, C. R.; Miller, S.; Tennyson, J.; Sutcliffe, B. T. *Mol. Phys.* **1992**, *76*, 1147.
(62) Li, L.; Lees, R. M.; Xu, L.-H. *J. Mol. Spectrosc.* **2007**, *243*, 219.
(63) Lees, R. M.; Li, L.; Xu, L.-H. *J. Mol. Spectrosc.* **2008**, *251*, 241.
(64) Horka, V.; Civis, S.; Xu, L.-H.; Lees, R. M. *Analyst* **2005**, *130*, 1148.
(65) Xu, L.-H.; Liu, Z.; Yakovlev, I.; Tretyakov, M. Y.; Lees, R. M. *Infrared Phys. Technol.* **2004**, *45*, 31.
(66) Berden, G.; Peeters, R.; Meijer, G. *Chem. Phys. Lett.* **1999**, *307*, 131.
(67) Cottaz, C.; Tarrago, G.; Kleiner, I.; Brown, L. R.; Margolis, J. S.; Poynter, R. L.; Pickett, H. M.; Fouchet, T.; Drossart, P.; Lellouch, E. *J. Mol. Spectrosc.* **2000**, *203*, 285.
(68) Kleiner, I.; Tarrago, G.; Brown, L. R. *J. Mol. Spectrosc.* **1995**, *173*, 120.
(69) Guelachvili, G.; Abdullah, A. H.; Tu, N.; Rao, K. N.; Urban, Š. *J. Mol. Spectrosc.* **1989**, *133*, 345.
(70) Kleiner, I.; Brown, L. R.; Tarrago, G.; Kou, Q.-L.; Picqué, N.; Guelachvili, G.; Dana, V.; Mandin, J.-Y. *J. Mol. Spectrosc.* **1999**, *193*, 46.
(71) Urban, Š.; Tu, N.; Rao, K. N.; Guelachvili, G. *J. Mol. Spectrosc.* **1989**, *133*, 312.
(72) Coy, S. L.; Lehmann, K. K. *Spectrochim. Acta* **1989**, *45A*, 47.
(73) Urban, Š.; Špirko, V.; Papoušek, D.; Kauppinen, J.; Belov, S. P.; Gershtein, L. I.; Krupnov, A. F. *J. Mol. Spectrosc.* **1981**, *88*, 274.
(74) Ziegler, L. D.; Hudson, B. *J. Phys. Chem.* **1984**, *88*, 1110.
(75) Nakanaga, T.; Kondo, S.; Saëki, S. *J. Mol. Spectrosc.* **1985**, *112*, 39.
(76) Margolis, J. S.; Kwan, Y. Y. *J. Mol. Spectrosc.* **1974**, *50*, 266.